# Numerical investigations of a prestressed pontoon wall subjected to ship collision loads

Yanyan Sha [a,*], Jørgen Amdahl [a]

[a] Centre for Autonomous Marine Operations and Systems (AMOS), Department of Marine Technology, Norwegian University of Science and Technology (NTNU), Norway

## Abstract

The paper presents a numerical investigation of the ship collision response for a floating pontoon. High fidelity finite element models of a container ship bow and a prestressed concrete pontoon wall are established. The effect of prestressing on the collision resistance of the pontoon is discussed. Integrated numerical simulations are conducted to study the structural deformation and energy absorption of the striking ship and the struck pontoon. The results are compared with the structural responses when a rigid ship collides with a deformable pontoon and a deformable ship collides against a rigid pontoon. Parametric studies are also carried out to investigate the effect of the pontoon wall thickness and the strength and dimension of the ship bulb. A dynamic punching shear check procedure that can be used in the preliminary design phase is proposed.

## 1. Introduction

The Norwegian Public Roads Administration (NPRA) is currently exploring the feasibility of constructing a new coastal highway along the west coast of Norway. Eight fjord-crossing installations will replace the existing ferry connections. Due to the wide and deep nature of the fjords, installations with fixed foundations are almost impossible to construct due to both technical and financial restrictions. Alternatively, novel floating bridges or tunnels have to be designed and constructed. For the floating bridge concepts, the bridge decks are typically supported by towers or columns resting on floating pontoons. The large-volume pontoons, which float at the sea surface level, are at risk of accidental ship collisions. The potential collision loads may cause damage to the pontoon wall and lead to subsequent flooding in the pontoon compartments. This can pose a significant threat to the safety of the floating bridge. Therefore, the collision resistance of the pontoons should be carefully evaluated to prevent progressive collapse of the bridge due to the collision-induced flooding in the pontoon.

Many previous studies have been reported on ship collision analysis. The earliest attempt for ship-ship collision investigation was conducted by Minorsky (1958). Based on this work, an empirical relationship between the volume of damaged material and the absorbed energy was proposed. Later, Woisin (1980) modified Minorsky's method and proposed a new formula based on a number of high energy collision tests. In the 1990s, Pedersen et al. (1993) and Amdahl and Eberg (1993) investigated ship-ship collisions and ship collision with offshore structures. Tabri et al. (2009) proposed an analytical model for ship collision analysis based on full-scale experiments. More recently, finite element (FE) methods have been widely used in analysing ship collision with other ships and offshore structures (Liu, 2017; Sun et al., 2015; Travanca and Hao, 2014). These works have offered good insights into the large displacement structural behaviour during a collision. Several widely used codes and guidelines, such as AASHTO (1991), Eurocode (1998) and NORSOK (2007), provide simplified formulae for estimating the collision loads.

However, most of the previous studies focus on ship-ship collision and ship collision with offshore structures. The literature on ship collision with bridges is limited. Yuan and Harik (2005; 2008, 2009), Consolazio et al. (2008; 2006; 2003, 2005; 2015), and Sha and Hao (2012, 2013, 2015) investigated barge collision with bridge piers. The vessel models in these analyses are typically barges travelling in inland waterways. The barges have much smaller bows compared with seagoing ships. In addition, ships normally have a larger displacement and travel faster (Kang et al., 2017). This means ship-induced collisions will easily exert a much larger demand for strain energy dissipation in the bridge structures. For ship-bridge collision, Fan and Yuan (2014) numerically investigated the collision response of a bridge pile cap considering soil-structure interaction. Later, Fan et al. (2016) proposed an approach to determining the dynamic ship-impact load based on the ship bow force-deformation relationship. The equations for



Corresponding Author: Yanyan Sha
yanyan.sha@ntnu.no

estimating the load duration and the time history of ship deformation were analytically derived. However, the structural deformation of the bridge components was ignored in the analysis.

In numerical ship-ship collision analyses, it is commonly assumed that the relatively stronger striking ship bow is rigid while the struck ship side structure is deformable. In ship-bridge collision analyses, the ship bow is typically modelled as a deformable structure and the reinforced concrete bridge pier is treated as a rigid body. While such assumptions simplify the modelling and simulation efforts, the idealization can sometimes lead to inaccurate results as the structural damage and energy dissipation of the bridge structure are neglected (Sha and Hao, 2012). It is necessary to conduct integrated analyses, which account for the deformation of both the striking ship and the struck bridge. For ship collision with floating bridges, this integrated analysis is deemed to be more critical as the water-tightness of the floating structure should be carefully checked (Sha and Amdahl, 2016). If a pontoon endures excessive damage, the water-tightness may not be maintained. Flooding of the pontoon may lead to collapse of the bridge superstructures.

In the paper, finite element models of a container ship bow and a prestressed concrete pontoon wall are presented. The prestress in the pontoon is included through a dynamic relaxation analysis. The effect of prestress on the collision resistance of the pontoon is discussed. Integrated numerical simulations are conducted to study the structural deformation and energy absorption of the striking ship and the struck pontoon. Parametric studies are carried out to investigate the effect of the pontoon wall thickness, the strength and dimension of the ship bulb. A punching shear check procedure that can be used in the preliminary design phase is proposed.

# 2. Pontoon model

The cable-stayed continuous floating bridge concept is shown in Figure 1. The cable-stayed main span in the middle is supported by two towers resting on two main pontoons. On each side of the main span, the continuous deck girder sits on nine small pontoons at both sides of the bridge. The waterway below the 450 m long cable-stayed middle span is designed as the navigation channel for large container and cruise ships. The two main pontoons are therefore especially exposed to ship collisions. In addition, they are more critical regarding the overall response of the whole bridge. Hence, the focus is placed on the collision resistance of the main pontoons in this study.

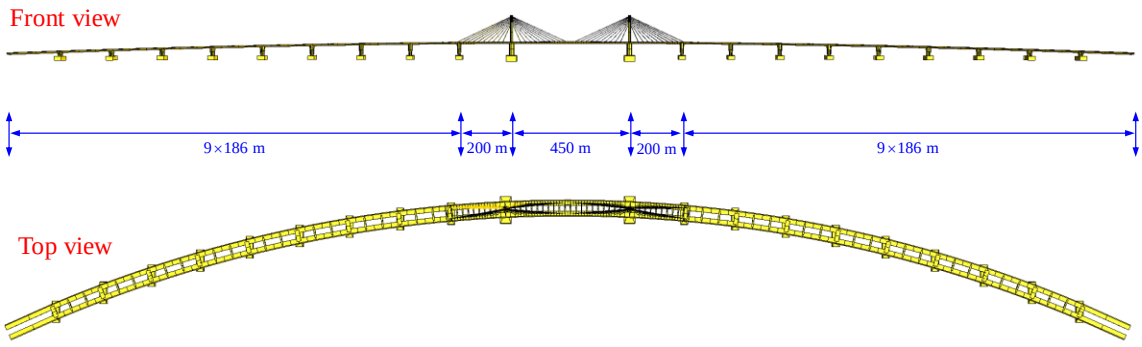


Figure 1. The floating bridge concept.

## 2.1 Pontoon wall configuration

The two main pontoons have the same dimension of 100 m in length and 40 m in width. The height of each pontoon is 20 m including a freeboard of 4 m. The pontoon dimensions are illustrated in Figure 2. The pontoon is divided into many compartments so that the damage of one or two compartments will not lead to excessive flooding. A finite element model based on this prototype is developed for the collision analysis. In order to limit the modelling effort and to reduce the computational time, only the front wall of the first middle compartment in the main pontoon was modelled in detail for the head-on collision scenario as indicated by the dashed area in Figure 2. Moreover, it was not necessary to model the whole pontoon as most of the structure is far away from the impact region and thus not expected to have any influence on the local collision response of the front wall.

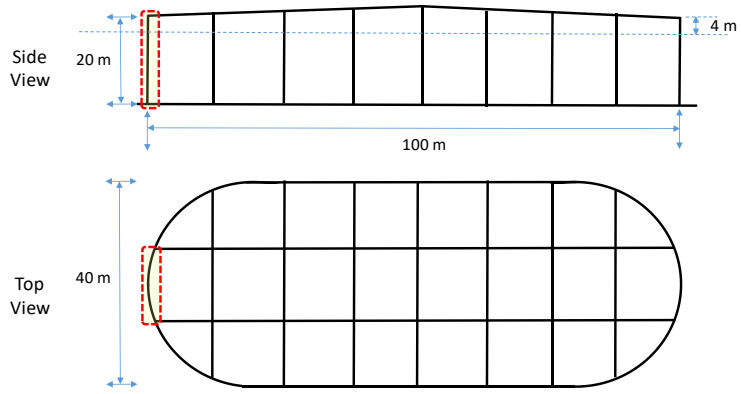


Figure 2. Dimensions of the main pontoon.

The pontoon wall is constructed of prestressed reinforced concrete. In order to accurately model the structural strength, detailed modelling was applied to the concrete, reinforcements and tendons in the pontoon, as shown in Figure 3. The 0.9 m thick concrete wall was modelled with 8-node solid elements. Two layers of reinforcement were embedded inside of the concrete cover of the pontoon wall. The diameter of the rebar and the stirrup is 15 mm and 8 mm, respectively. The prestress in the concrete is provided by tendons made by strands of high strength steel wires. The diameter of the vertical and transverse tendons is 90 mm and 70 mm, respectively. The tendons are placed between two layers of reinforcements. The reinforcements and tendons were both modelled by circular beam elements.

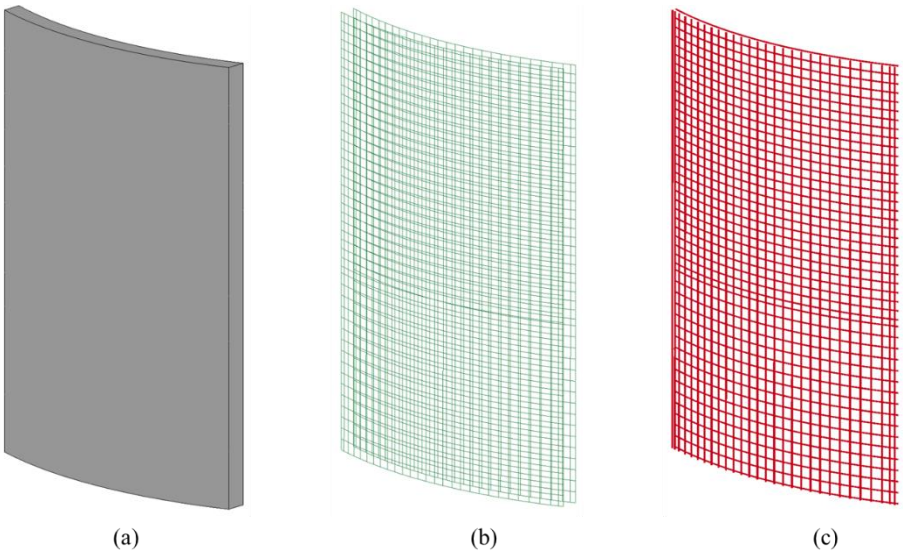


Figure 3. FE model of the pontoon wall: (a) concrete, (b) rebar and stirrup, and (c) tendon.

## 2.2 Material modelling

The material model MAT_72R3 in LS-DYNA, which can simulate concrete damage under impact and collision loads with good accuracy (Sha and Hao, 2012, 2013) was used for the concrete material in the pontoon. This material model has been widely employed to model the dynamic behaviour of concrete including plasticity and damage softening after failure. The concrete has a compressive strength of 60 MPa and the failure strain is set to 0.1 (Sha and Hao, 2012).

The elastic-plastic material model MAT_PIECEWISE_LINEAR_PLASTICITY was employed to model the steel reinforcements and tendons in the pontoon. The reinforcements are made of normal mild steel with a yield stress of 275 MPa. The tendons are typically designated CONA-CMI-BT 1306-150 and made by high strength steel strands with a yield stress of 1860 MPa. Characteristic properties of all materials are tabulated in Table 1.

Any strain rate effect was neglected in the study for both steel and concrete materials. The main reason is that the strain rate effect is relatively small in the present case and is rather uncertain and challenging to analyze properly as discussed by M Storheim and J Amdahl (2017). It is normally conservative to neglect it for the struck pontoon, but may be unconservative for the crushing force of the bow, which represents the "action". It is also likely that the two effects may cancel each other to some extent.

Table 1: Material parameters for the pontoon.

| Materials | Items | Values |
|---|---|---|
| Concrete | Density | 2400 kg/m$^3$ |
| | Poisson's ratio | 0.2 |
| | Compressive strength | 60 MPa |
| | Failure strain | 0.1 |
| Steel (Reinforcements) | Density | 7850 kg/m$^3$ |
| | Poisson's ratio | 0.3 |
| | Young's modulus | 2.1E11 |
| | Yield stress | 275 MPa |
| | Failure strain | 0.35 |
| Steel (Tendons) | Density | 7850 kg/m$^3$ |
| | Poisson's ratio | 0.3 |
| | Young's modulus | 2.1E11 |
| | Yield stress | 1860 MPa |
| | Failure strain | 0.35 |

## 2.3 Prestress modelling

For floating pontoons, it is critical to ensure the water-tightness during their service life. Conventional pontoons are made of reinforced concrete (RC). Due to the low tensile strength of concrete, RC floating structures are vulnerable to tensile cracks, which may develop under permanent hydrostatic loadings. Therefore, significant efforts are required for the constant repairing of surface cracks to ensure the water-tightness of the pontoons during their service life. Otherwise, the surface cracks may eventually result in water leakage and pontoon flooding.

To save cost related to repair, prestressed concrete (PC) may be used instead of reinforced concrete. Compared with RC structures, the tensile strength of PC structures is greatly improved by the introduction of initial compressive stresses. In this study, the pre-tensioning method is used to apply the initial stress to the pontoon wall. In LS-DYNA, three approaches may be used to tension the tendons and pre-stress the concrete. They include the static implicit method, the transient explicit method and the dynamic relaxation method (Schwer, 2016). In this work, the dynamic relaxation technique is utilized. An advantage of the dynamic relaxation method is that one can control the convergence of the analysis to make sure that the result is close to the desired quasi-static state. This can be achieved by plotting the convergence factor and energy curves after the dynamic relaxation analysis is finished.

To introduce prestress in the concrete, the tendons are first tensioned to the desired axial force level. Nodal loads are applied at both ends of the tendons through a dynamic relaxation analysis. The tensile stress in the tensioned tendons is stored and written into a DYNAIN file for the concrete pre-stressing in the second step. The convergence of the dynamic relaxation analysis is checked by the convergence factor curve and total energy curve as shown in Figure 4. The axial forces in the vertical and horizontal tendons after convergence are shown in Figure 5 (a).

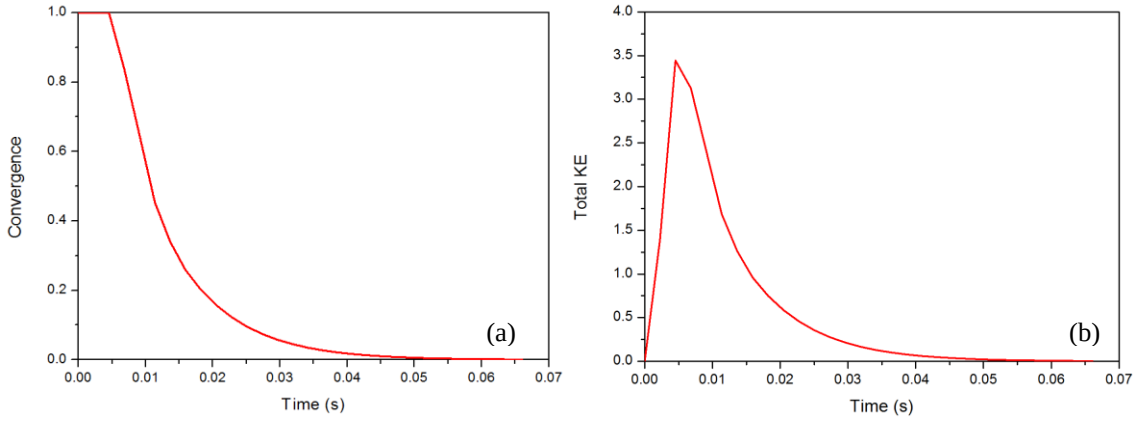


Figure 4. (a) Convergence curve, and (b) energy curve.

The DYNAIN file outputted from the tendon-tensioning analysis is included in the input file for concrete pre-stressing. A dynamic relaxation analysis is conducted to transmit the tension stresses in the tendons to compressive stresses in the concrete. To make sure the stress is correctly transmitted, the tendon elements and concrete elements should be properly coupled. There are different methods to ensure proper bonding between tendons and concrete including shear nodes, using 1D element, and defining constraints between tendons and concrete. In this study, the tendon beam elements and concrete solid elements are coupled by sharing nodes. The compressive stresses in the concrete after convergence are shown in Figure 5 (b).

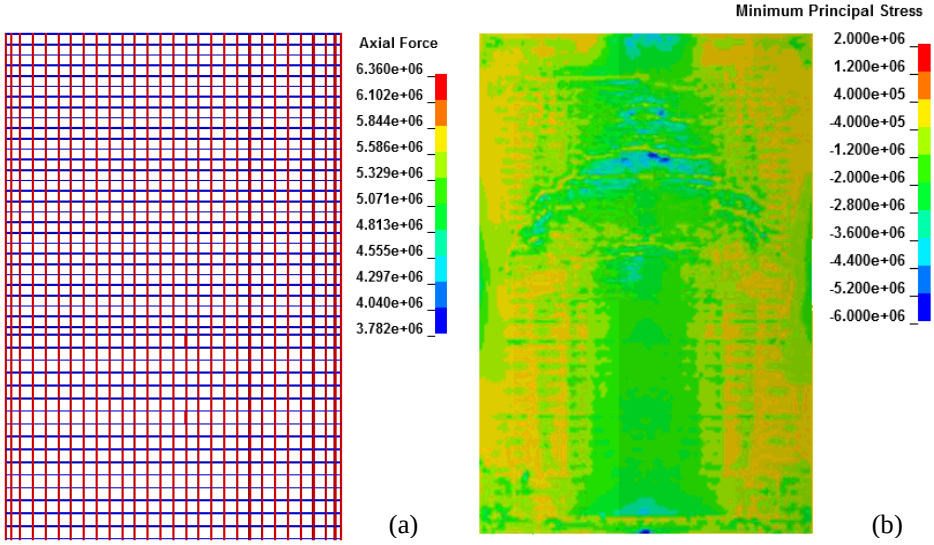


Figure 5. (a) Axial force in the tendons after tendon tensioning, and (b) compressive stress in the concrete after prestressing.

# 3. Ship bow model

The ship bow model used in this study is based on the container ship shown in Figure 6 with a displacement of 20,000 tons. The ship has an overall length of 166.62 m and a moulded breadth of 27.4 m. The depth and the scantling draught of the ship are 13.2 m and 9.6 m, respectively. As shown in Figure 6, the first 20 meters of the ship bow structures are modelled. This is considered sufficient to avoid influence of boundary conditions for the crushing range analyzed. The decks, stringers and transverse frames are included in addition to the outer shell panels. The vertical stiffeners have a spacing of 0.6 m. The thickness of the steel components in the ship bow varies from 7.5 mm to 20.5 mm.

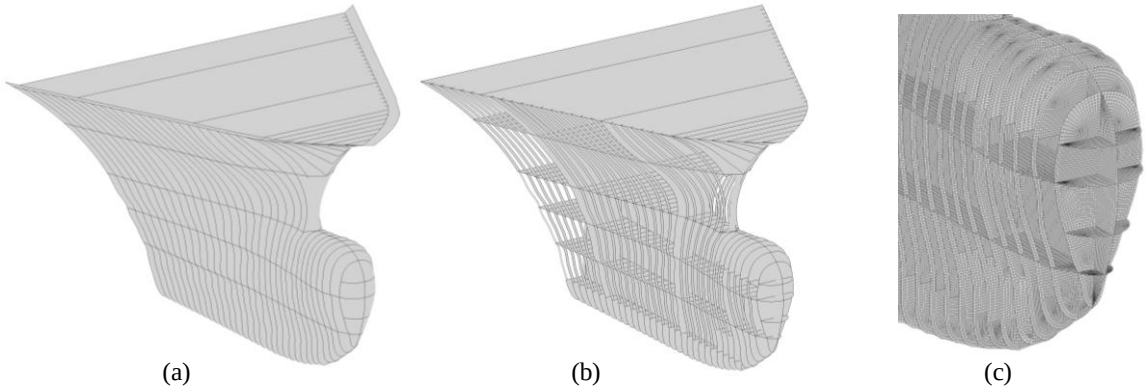

(a) (b) (c)

Figure 6. FE model of the ship bow, (a) outer hull, (b) internal structure and (c) structural density.

## 3.1 Element and mesh

The four-node Belytschko-Lin-Tsay shell element with five integration points is used in modelling the ship bow structure because of its computational efficiency. The mesh size not only has a critical influence on the accuracy and reliability of the results, but is also related to the computational time. The balance between simulation accuracy with respect to structural resistance, fracture prediction and computational efficiency should be maintained. In this study, the element size is generally set to 80 mm, which gives a length-thickness ratio in the acceptable range of 4-10 (Kulzep and Peschmann, 1999). The mesh size for the pontoon is similar to that of the ship.

## 3.2 Material modelling

Material modelling is also a critical aspect in ship collision analysis. A verified power-law hardening model is used to model the steel material in the container ship (Alsos et al., 2009). This material is assumed to have isotropic plastic properties and the yield condition is based on plane stress $J_2$ flow theory. The equivalent stress-strain relationship is represented by a modified power-law formulation, which includes the plateau strain to delay the onset of hardening. The plasticity formulation is assumed to be strain rate independent

The Rice-Tracey-Cockcroft-Latham criterion (RTCL) is used to model the material fracture. It considers stress triaxiality to distinguish between shear and tension dominated damage. Fracture is initiated once the accumulated damage reaches a critical level. The criterion is mesh scaled which has been proved to give a good simulation of steel fracture (Alsos et al., 2009). The container ship is fabricated in mild steel with a yield stress of 275 MPa. Detailed material parameters are tabulated in Table 2.

Table 2: Material parameters for the ship bow.

| Materials | Items | Values |
|---|---|---|
| Steel | Density | 7890 kg/m$^3$ |
| | Young's modulus | 210 GPa |
| | Poisson's ratio | 0.3 |
| | Yield stress | 275 MPa |
| | Strength index | 740 MPa |
| | Strain index | 0.24 |

## 3.3 Pressure-area relationship of ship bulb

For the preliminary collision design of the pontoon, an impact pressure-contact area relationship can be utilized. Storheim and Amdahl (2014) calculated the average pressure-contact area relationship for a modern supply vessel of 7500-ton based on nonlinear FE simulations. An empirical equation between the impact pressure and the contact area was proposed as

$$P = 12 \cdot A^{-0.7}, \tag{1}$$

where $P$ and $A$ are the average impact pressure and the contact area, respectively.

Similarly, the pressure-area relationship is also obtained in the current study by crushing the ship bulb against a rigid wall. Local contact pressures over subsets of the total contact area were calculated at different stages of deformations of the bow. The results are plotted in Figure 7. A fitted curve is proposed and plotted together with the simulation results in the figure. The fitted curves can be represented by

$$P = 18 \cdot A^{-1.5} . \tag{2}$$

Compared with the bulb of the supply vessel bow described by Storheim and Amdahl (2014), the container ship bulb is much stronger. Naturally, a higher pressure is observed in the early stage when the contact area is small. To account for this early-stage high pressure, a relatively large pressure coefficient of 18 and a small power coefficient of -1.5 is proposed as shown in Eq. 2. After the strong ship bulb head is crushed, the contact pressure is dominated mainly by the crushing resistance of the stiffened hull and the horizontal decks. The pressure-area relationship at this stage is then in the similar range as the supply vessel.

It is worth mentioning that the local high pressures have very limited durations and are continuously changing position. Hence, for the bulb collision with a concrete pontoon wall, it is possible that the concrete wall will entirely resist or undergo small nonlinear deformations during the short-lived contact forces. Further, any partial failure of the concrete wall is likely to relax the contact force. These aspects have so far not been addressed.

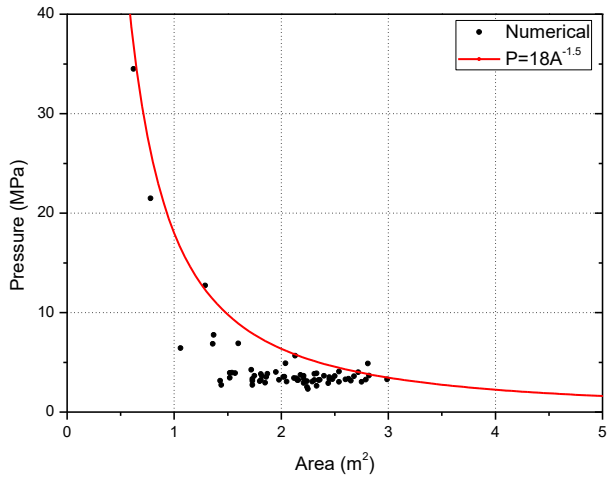


Figure 7. Pressure-area relationship for bulb collision against a rigid wall.

# 4. Numerical simulations

To speed up the simulations, the ship collides against the pontoon wall at a constant speed of 10 m/s. This is considered reasonable with respect to avoiding significant dynamic buckling effects (while strain rate is not considered). The actual damage is determined by the evaluation of the energy dissipation relationships. The nodes at the four sides of the pontoon wall are fixed in all degrees of freedom. This fixed boundary condition is considered appropriate as there are top and bottom slabs and transverse internal walls which support the wall portion we have modelled as shown in Figure 2. Since the impacted area is sufficiently far away from the boundary, this fixed boundary condition will not influence the results significantly. Moreover, the pontoon response is dominated by the local punching shear while the flexural response is marginal as discussed in Section 4. The Automatic Surface to Surface Contact (ASTS) algorithm is used to model the interaction between the ship and the pontoon. The internal contacts of the ship bow are considered by defining the Automatic Single Surface Contact (ASSC) algorithm for all ship parts. The ASSC is also assigned to the concrete, reinforcements and tendons. For all contact types, the static and dynamic friction coefficients are set to 0.3 (Sha and Hao, 2012).

## 4.1 Structural deformation and impact force

Apart from the integrated ship-pontoon collision simulation (a deformable ship against a deformable pontoon), a deformable ship against a rigid pontoon and a rigid ship against a deformable pontoon are also simulated for comparison. The force-displacement curves for the three cases are plotted in Figure 8 and the structural deformations are illustrated in Figure 9.

In the integrated analysis, the collision force increases quickly to the first peak of 15 MN at 0.1 m displacement. A small drop occurs at this time instant due to the crushing failure of the concrete cover. The collision force then increases to 35 MN as more structural components in the ship bulb get in contact with the pontoon wall. A significant decrease in impact force follows as the horizontal deck and first vertical frame in the bulb buckles. After that, clear crests and troughs can be observed due to the continuous buckling and crushing of decks and collapse of vertical frames in the ship bulb. In general, the ship bow endures a large deformation in the bulb. The pontoon wall is generally intact during the whole collision process. This shows that the strength of the pontoon wall is higher than that of the ship bulb. The ship resistance determines the collision force history and the majority of the collision energy is dissipated through the deformation and damage of the ship bulb.

For deformable bow against a rigid pontoon, the evolution of the impact force follows the same pattern as the integrated analysis, but the variation between peaks and troughs is slightly larger in the first half of the deformation range. Thus, the flexibility of the wall smoothens the curves somewhat, but the average force remains the same. The structural response is also similar to that in the integrated analysis as the strength of the ship bulb dominates the collision process. The collision energy is only dissipated by deformation of the ship bulb in this case.

For rigid ship against a deformable pontoon wall, the force-displacement curve is completely different from the two other cases. The pontoon strength controls the force level. The peak force attains 35 MN and then quickly drops to a small value as the bulb penetrates the pontoon wall. Structural damage occurs only in the pontoon wall as shown in Figure 9 (c). The collision energy is dissipated through the failure of the pontoon wall. The ship bulb penetrates the pontoon wall in a very short time and the total energy dissipation is significantly lower than in the other two cases.

These results demonstrate the enormous importance that the resistance to the punching of the concrete wall plays. For the present case, it can be concluded that the pontoon behaves as if it had been dimensioned according to strength design principles (Norsok, 2004). An assessment based on a rigid ship bow would be very conservative and may lead to design problems.

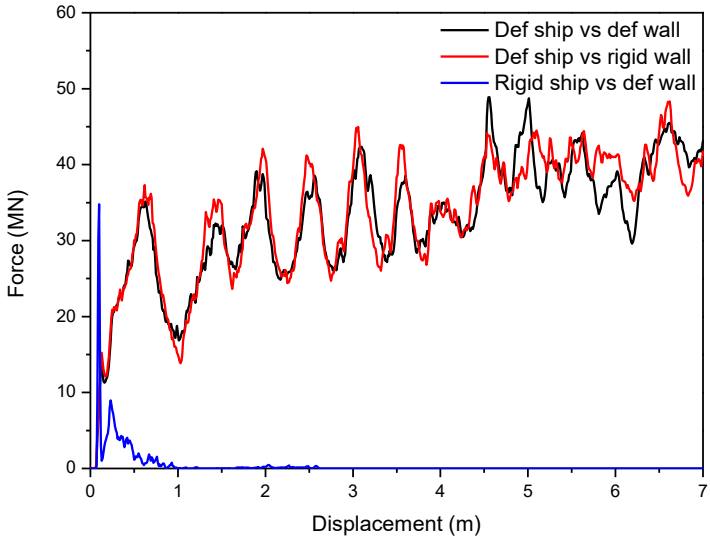


Figure 8. Impact force versus ship displacement.

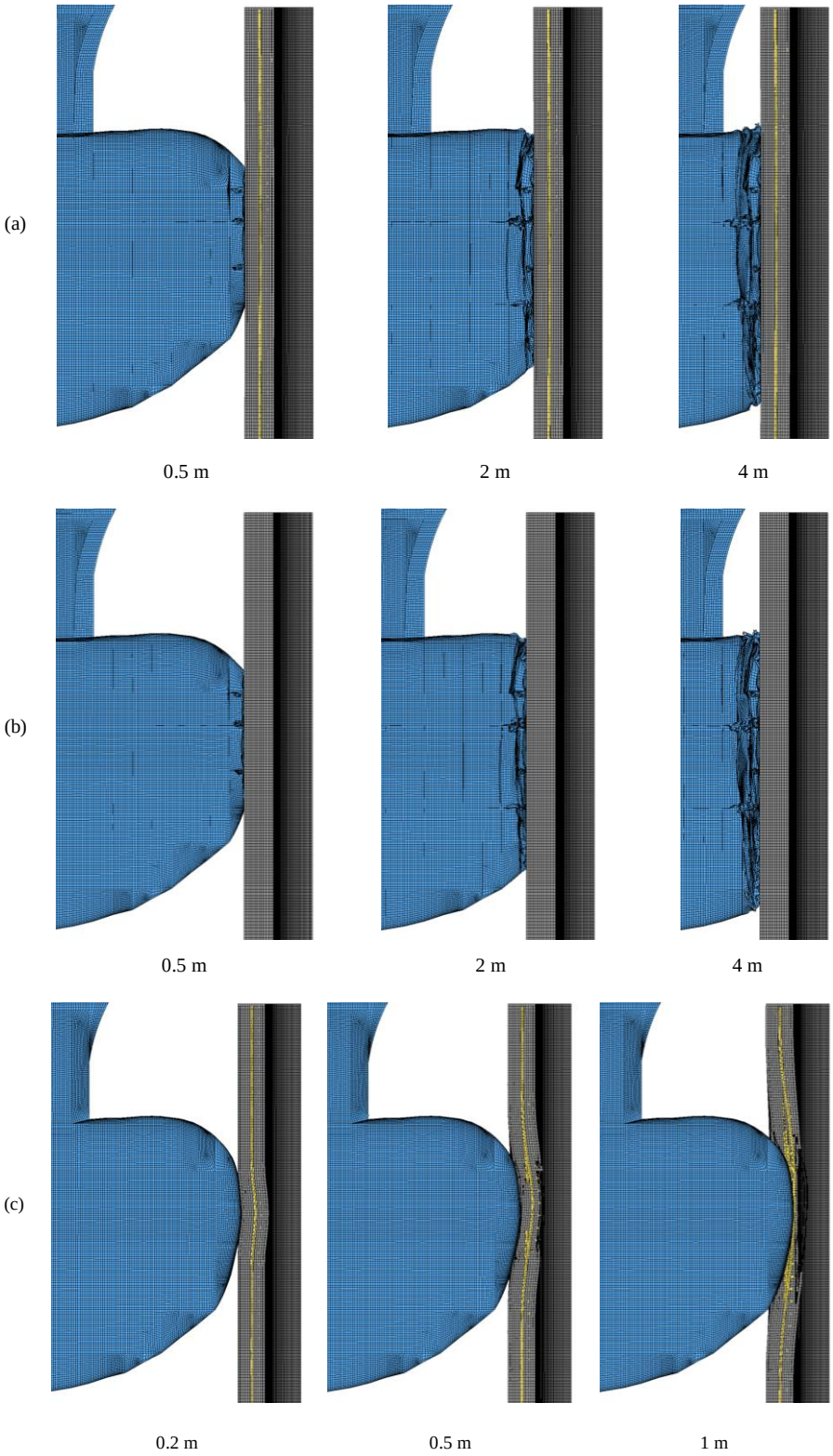


Figure 9. Structural deformation in the (a) integrated analysis, (b) deformable ship against rigid pontoon, and (c) rigid ship against deformable pontoon.

## 4.2 Effect of prestress

To investigate the effect of prestressing, a pontoon wall model without prestressing is developed. The response to the deformable bulb impact is compared with that for the prestressed pontoon wall.

The impact force time histories are compared in Figure 10 (a). Up to 0.55 s, the force curves are virtually identical as the bulb crushes and governs the collision force. At 0.55 seconds corresponding to approximately 5.5 m crushing of the bulb and when the forces reach a peak of 50 MN, the wall without prestressing is penetrated by the remaining part of the bulb. This is associated with a dramatic drop in the force level.

The axial stress in the rebar is compared in Figure 10 (b). For the prestressed wall, the axial stress is relatively low throughout the collision process because the pontoon remains intact. For the wall without prestressing, the axial stress in the rebar increases rapidly from 0.5 s and then drops quickly to zero. This is because the concrete cover suffers crushing damage that results in direct contact between the ship bulb and the reinforcements. Next, the rebar breaks due to a tensile fracture.

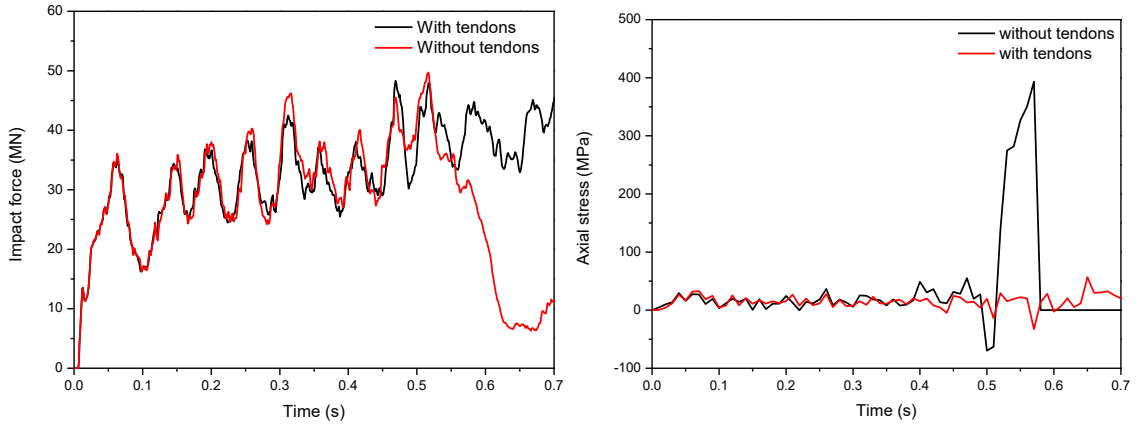


Figure 10. (a) Impact force, and (b) rebar stress.

Figure 11 shows that the bulb dissipates the majority of the collision energy in both cases up to the level of 160 MJ. However, the share of energy dissipation changes dramatically after 0.55 s when the pontoon without prestressing also starts to absorb energy. This corresponds to impact speed of 4 m/s for a 20,000-ton ship if all energy is dissipated as strain energy (Some energy may be transferred to kinetic energy of the pontoon and bridge). Thus, for a larger impact speed, the picture will change a lot. In addition to the change of energy distribution, flooding will take place in the non-prestressed pontoon.

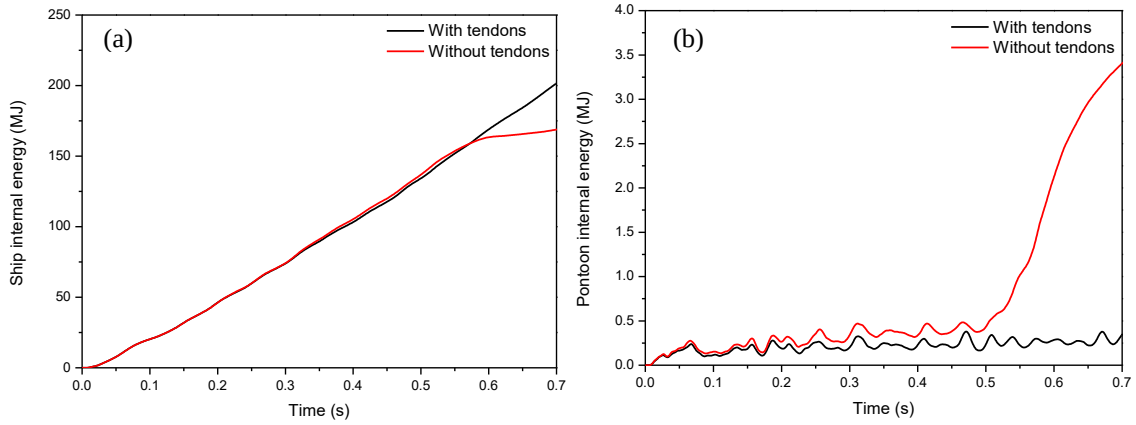


Figure 11. (a) Ship internal energy, and (b) pontoon internal energy.

The effective plastic strain contours of the pontoon wall with and without prestressing are illustrated in Figure 12. In the beginning, the contours are quite similar in both cases and large plastic strains concentrate

in the contact area. With prestressing, the pontoon maintains integrity during the whole collision process, i.e. no hole that will lead to flooding is created in the wall. Without prestressing, large strains develop in the lower part of the contact area at 0.4 s. Excessive damage occurs around the contact perimeter. The concrete wall is partly crushed and will allow flooding to take place. In both cases, the ship forecastle starts to contact the top of the pontoon wall at 0.6 s.

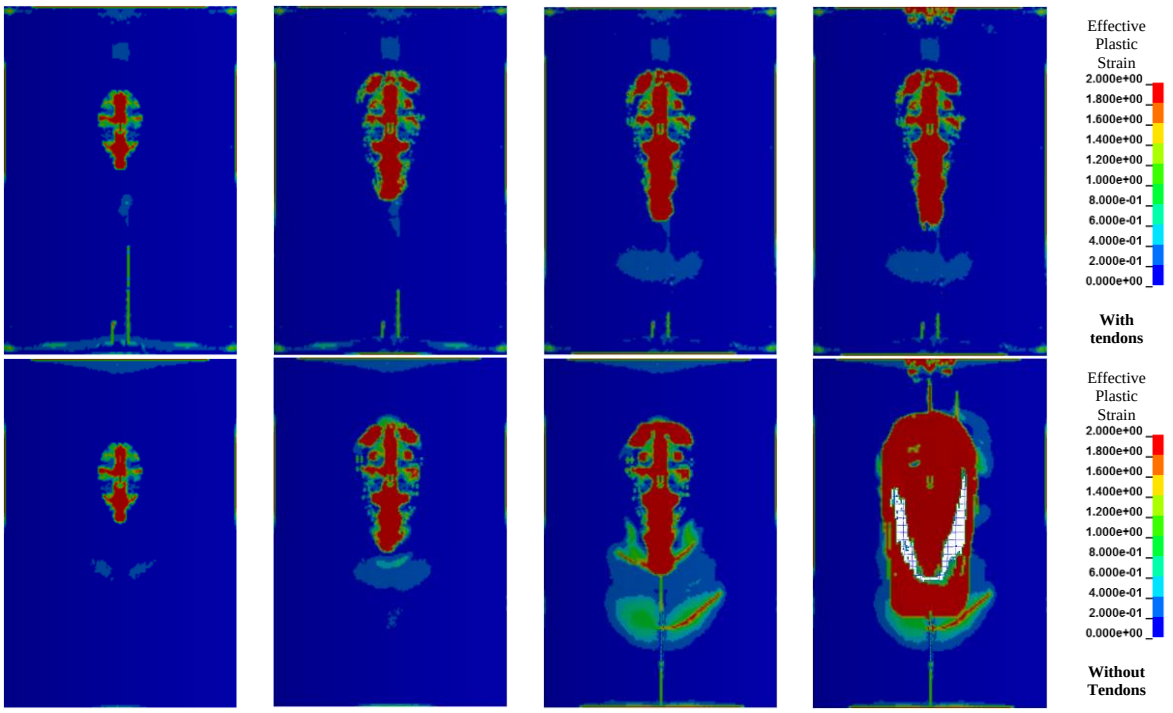


Figure 12. Strain contours of the pontoon wall with and without tendons.

## 4.3 Effect of pontoon wall thickness

To evaluate the effect of the pontoon wall thickness on the collision resistance, two analyses are conducted with thicknesses of 0.7 m and 0.8 m and compared with the original design of 0.9 m thickness. In all cases, the pontoon walls are prestressed.

The force-displacement curves for the different wall thicknesses are shown in Figure 13. When the wall thickness is 0.8 m or less, the pontoon has insufficient capacity to resist the collision from the bulb for the deformation range analyzed. A thinner wall fails earlier and results in a lower energy absorption ability prior to flooding. The energy dissipated for 0.8 m thickness is about 60 MJ while only 18 MJ collision energy is dissipated for the 0.7 m thick wall. The corresponding impact speed considering all energy to be dissipated as strain energy is 2.5 m/s and 1.3 m/s.

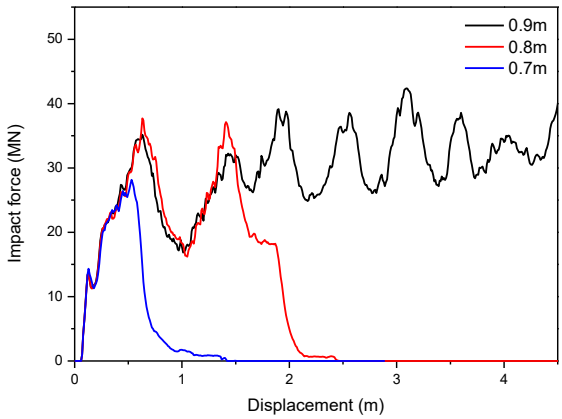


Figure 13. Force-displacement curves of prestressed pontoons with various wall thickness.

Figure 14 shows the structural damage in the three cases. The bulb penetrates the pontoon wall with very little deformation with a wall thickness of 0.7 m. The crushing of the bulb before penetration is more pronounced for the 0.8 m thick wall while the pontoon with a wall thickness 0.9 m can resist the impact with very limited spalling damages on the surface. This shows that the structural damage is very sensitive to the relative strength of the ship bulb and the pontoon wall. The major deformation switches from the ship to the pontoon when the wall thickness is reduced from 0.9 m to 0.8 m or less.

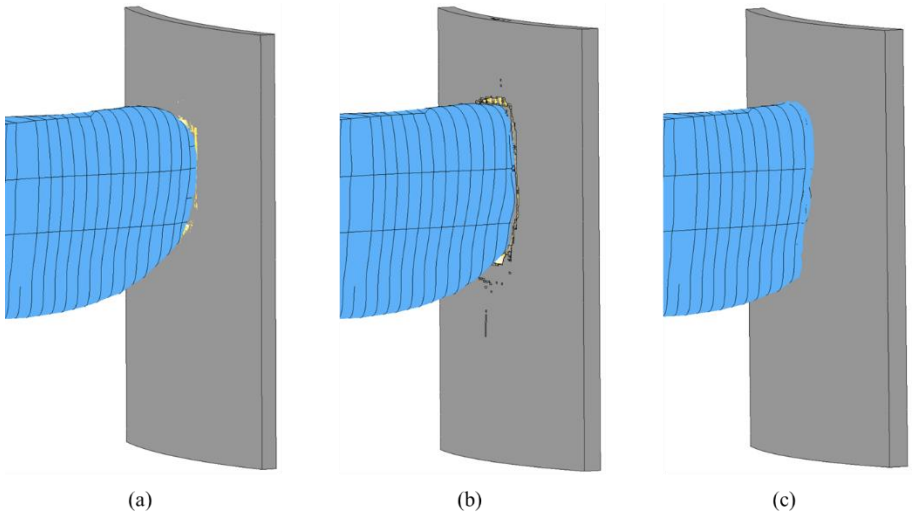


Figure 14. Structural damage for (a) 0.7 m thick pontoon wall at 1 m ship displacement and (b) 0.8 m thick pontoon wall at 2 m ship displacement, and (c) 0.9 m thick pontoon wall at 3 m ship displacement.

## 4.4 Punching shear considerations

When the pontoon strength is smaller than the ship bulb, a typical punching shear failure takes place in the pontoon wall (see Figure 14 (a) and (b)). According to Eurocode 2 (2004), the punching shear stress for a reinforced concrete slab can be calculated based on the impact loads and slab dimensions. The shear stress should be checked at the loading and the control perimeters as shown in Figure 15.

The shear stress at the loading perimeter should not exceed the shear capacity of the structure as given in the following equation:

$$v_{\mathrm{Ed}} = \beta V_{\mathrm{Ed}} / (u_0 d) < v_{\mathrm{Rd,max}} = 0.4 \times 0.6 \cdot (1 - \frac{f_{\mathrm{ck}}}{250}) f_{\mathrm{cd}}\,, \tag{3}$$

where $v_{Ed}$ is the numerically calculated shear stress, $v_{Rd,max}$ is the shear capacity at the loading perimeter. $\beta = 1.15$ is the factor accounting for eccentricity and $V_{Ed}$ is the shear force. $u_0$ is the perimeter of the loaded area and $d$ is the effective depth of the wall. $f_{cd} = 60MPa$ and $f_{ck} = 50MPa$ are the design and cylinder compressive strength of the concrete.

Similarly, the shear stress at the basic control perimeter should be checked by

$$v_{Ed} = \beta V_{Ed} / (u_1 d) < v_{Rd,c} = C_{Rd,c} k \left(100 \rho_1 f_{ck}\right)^{1/3}, \quad (4)$$

where $v_{Rd,c}$ is the shear capacity at the basic perimeters and $u_1$ is the perimeter of the basic control area. $C_{Rd,c} = 0.12$ and $k = 1 + \sqrt{0.2 / d} \le 2$ are the size coefficients. $\rho_1 \le 0.02$ is the reinforcement ratio.

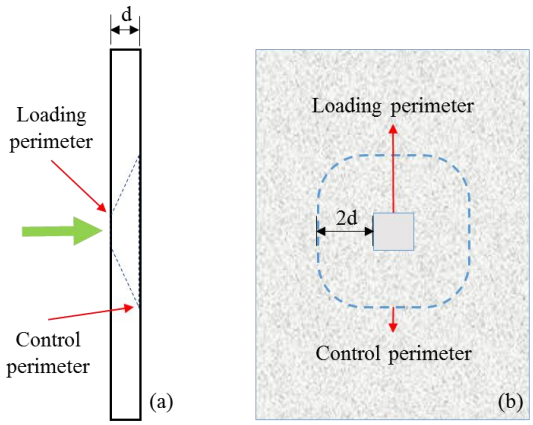


Figure 15. The contact perimeter and the control perimeter; (a) side view, and (b) front view.

The punching shear check method is applied herein for ship collision with the prestressed pontoon wall. The shear force in Eq. 3 and 4 are taken as the impact load obtained from the numerical simulation. As the impact force is time-dependent, the numerically calculated shear stresses also vary with time. Hence, a 'dynamic' punching shear check with respect to time is plotted for different wall thickness as shown in Figure 16. The shear stresses at the loading and the control perimeters calculated based on the simulation results are then compared with the code specified shear capacities.

The shear stress history and the shear capacity for a 0.9 m thick pontoon wall are shown in Figure 16 (a). The shear stress at the loading perimeter is much lower than the capacity most of the time, except for the beginning when the calculated shear stress exceeds the capacity. At this stage, the contact area is small and the loading is short-lived, so it does not lead to punching failure of the pontoon wall. At the control perimeter, the calculated shear stress is fluctuating around the shear capacity.

For the 0.8 m thick pontoon wall, the shear stress at the loading perimeter is also much lower than the capacity. At the control perimeter, the shear stress becomes consistently larger than the capacity after 0.22 s, (see Figure 16 (b)) and the pontoon wall fails. This predicted failure time agrees well with the impact force time history as shown in Figure 13.

Figure 16 (c) shows that the 0.7 m thick pontoon wall still has sufficient shear capacity at the loading perimeter. The shear stress at the control perimeter is, however, larger than the shear capacity after around 0.07 s. This also agrees well with the impact force time history in Figure 13.

Generally, the shear capacity at the loading perimeter is sufficient for the current ship collision load. However, the shear stress is close to or exceeds the capacity at the control perimeter. These results illustrate that punching shear check approach can be efficiently used in the preliminary design phase.

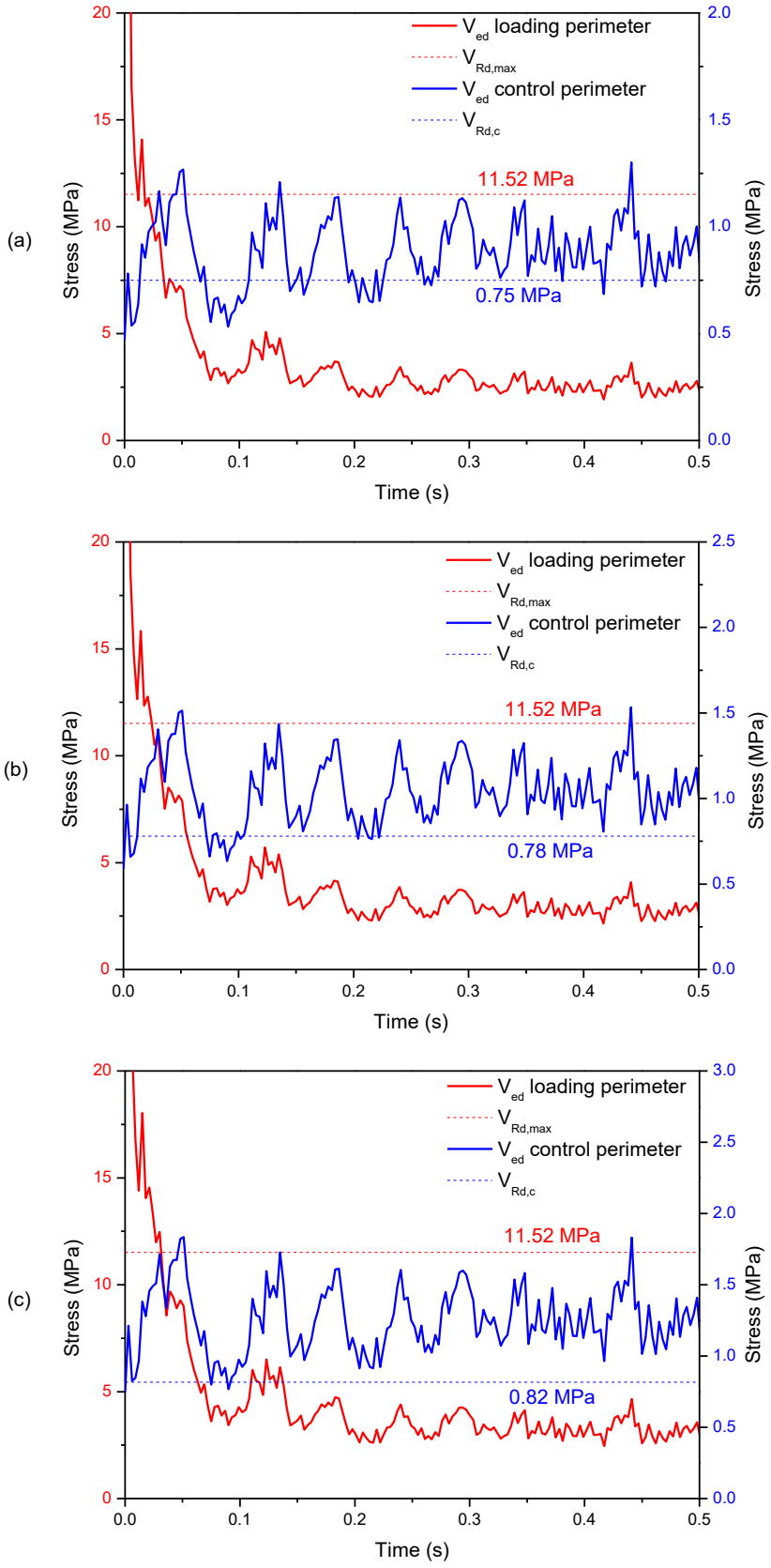


Figure 16. Punching shear design, (a) 0.9 m (b) 0.8 m and (c) 0.7 m thick pontoon wall.

## 4.5 Effect of ship bulb type

The above analysis is conducted with a ship bow model for a 20,000-ton container ship. To cover a wider range of ship bows, two additional bow models were developed. One is a cruise ship of a similar displacement, but it has a lower bulb height of 5.5 m as shown in Figure 17 (b). The ship was constructed of normal strength steel with a yield stress of 275 MPa and the plate thickness is in the range of 9-14.5 mm. Figure 17 (c) shows the bow model of an ice-strengthened container ship, which was constructed of high strength steel with a yield stress of 390 MPa and the steel plate thickness is typically in the range of 16-25 mm. The ship models are illustrated in Figure 17 and the corresponding dimensions of the three bulbs are listed in Table 3.

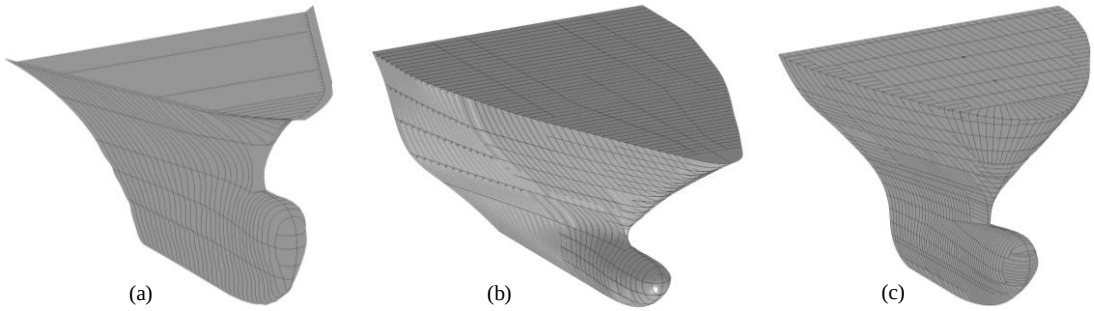


Figure 17. FE models of the three ship bows; (a) container ship, (b) cruise ship, and (c) ice-strengthened container ship.

Table 3: Dimensions of the three ship bulbs (m).

| Ship type | Overall model length | Bulb height | Bulb width |
|---|---|---|---|
| Container ship (Fig. 17a) | 20 | 8.5 | 3.5 |
| Cruise ship (Fig. 17b) | 30 | 5.5 | 2.9 |
| Ice-strengthened ship (Fig. 17c) | 17 | 6.8 | 2.8 |

Crushing simulation against a rigid wall is first conducted and the force-crush depth relationships are compared for the three ship bows as shown in Figure 18. The cruise ship and the normal container ship have a maximum force level of 25 MN and 50 MN, respectively. For the ice-strengthened container ship, the force level is much higher and reaches 80 MN. Thus, the three bow models cover a wide range of ship bow strength and it is interesting to compare the response of the pontoon to these bow collisions. It should be noted that the force-crush depth curves are only presented up to 5 m crush depth. Upon further crash, the force level may vary depending on the structural configuration in the ship bow.

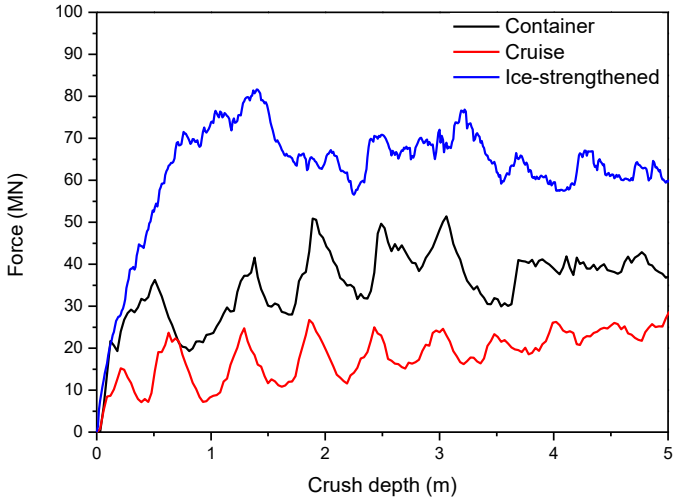


Figure 18. Force-crush depth curves of the three ship bulbs.

Integrated analyses are carried out for the pontoon wall with a thickness of 0.9 m. The ship bows have an initial velocity of 10 m/s in all three cases. Ship and pontoon wall damages are compared in Figure 19 and Figure 20. It comes as no surprise that the bulb of the cruise ship deforms completely as it is weaker than the container vessel. The pontoon wall remains generally intact. In the ice-strengthened vessel case, the bulb suffers very limited deformation while a large punching hole is created in the pontoon wall upon contact. Very limited (less than 2 MJ) energy is dissipated when the pontoon wall is punched through. Further investigation would be needed for the damage stability with flooded compartments and the global response of the whole bridge.

The proposed 0.9 m thick pontoon wall with prestressing represents a strength design concept with respect to collisions from normal strength ship bows with a displacement in the range of 20,000 to 40,000 tons. However, this is no longer the case if ice-strengthened ships pass the bridge. The major damage will typically switch from the ship bulb to the pontoon. Moreover, if penetration of one compartment is not sufficient to dissipate all the collision energy, several compartments must be involved. This could, in turn, lead to pontoon sinking or overturning that could put the global bridge stability in jeopardy.

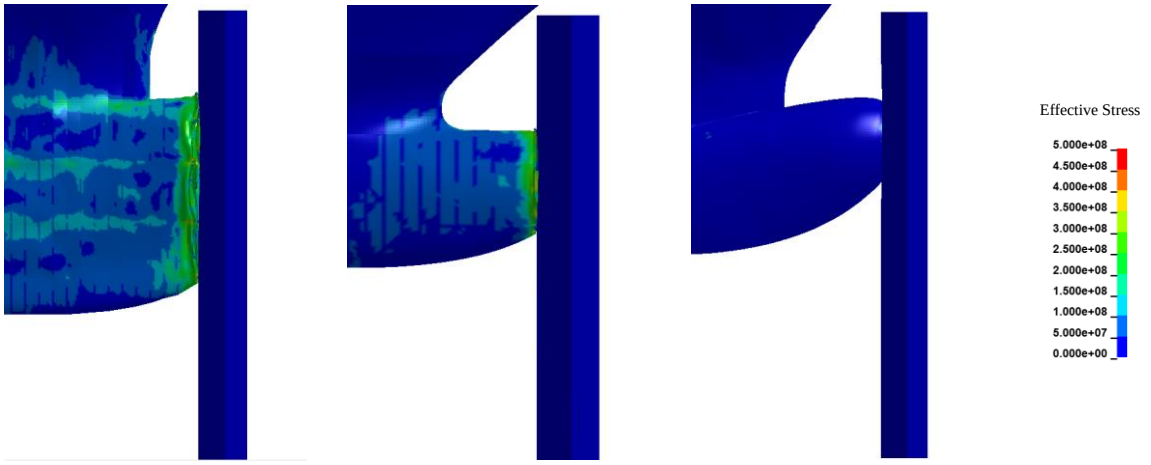


Container Cruise Ice-strengthened

Figure 19. Ship bow damages.

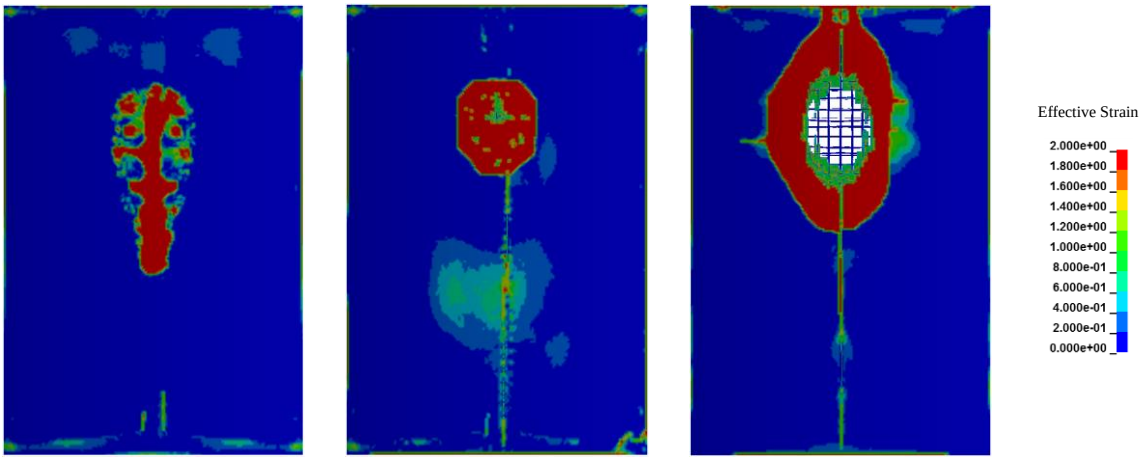


Container Cruise Ice-strengthened

Figure 20. Pontoon wall damage.

# Conclusions

Finite element models of a prestressed pontoon wall for a floating bridge and the bow of a 20,000-ton container ship were established and numerical simulations were conducted to investigate the response of the ship and pontoon during a collision. The findings from the current study can be summarized as follows:

The introduction of a prestress in the pontoon wall will not only help to ensure the water-tightness of the structure but also increases the collision resistance. A 0.9 m thick pontoon remained generally intact under the collision of the container ship bow. In the case studied, it would be very conservative to assume the ship bow to be rigid because the energy dissipation was mostly taking place in the ship bow.

The results from the simulations were compared with the punching shear checks formulated in Eurocode 2. It was found the shear capacity at the loading perimeter was normally sufficient. The shear stress at the control perimeter tends to be more critical. The requirements largely confirmed the results from the numerical simulations and showed that the procedure may be efficiently used in the preliminary design based on the force-deformation and contact area-deformation curves for the design collision event.

The structural damage was very sensitive to the relative strength of the ship bulb and the pontoon wall. The major deformation switched from the ship to the pontoon when the pontoon wall thickness was reduced from 0.9 m to 0.8 m or less.

The simulations showed that the pontoon could be considered dimensioned according to strength design principles as far as the collisions with normal strength ship are concerned. However, the major structural failure can easily switch from the ship to the pontoon if an ice-strengthened ship is involved. The transition between different design regimes is very sensitive to the relative strength, and it is important to critically evaluate the collision scenario and adopt accurate analysis methods in the bridge design process, notably, if strength design shall apply.

# Acknowledgement

This work was supported by the Norwegian Public Roads Administration (project number 328002) and in parts by the Research Council of Norway through the Centres of Excellence funding scheme, project AMOS (project number 223254). The support is gratefully acknowledged by the authors.

# References

AASHTO, 1991. Guide Specification and Commentary for vessel collision design of highway bridges. American Association of State Highway and Transportation Officials, Washington, DC.

Alsos, H.S., Amdahl, J., Hopperstad, O.S., 2009. On the resistance to penetration of stiffened plates, Part II: Numerical analysis. International Journal of Impact Engineering 36 (7), 875-887.

Amdahl, J., Eberg, E., 1993. Ship collision with offshore structures, Proceedings of the 2nd European Conference on Structural Dynamics (EURODYN'93), Trondheim, Norway, June, pp. 21-23.

Consolazio, G., Davidson, M., 2008. Simplified dynamic analysis of barge collision for bridge design. Transportation Research Record: Journal of the Transportation Research Board (2050), 13-25.

Consolazio, G.R., Cook, R.A., McVay, M.C., Cowan, D., Biggs, A., Bui, L., 2006. Barge impact testing of the St. George Island causeway bridge. Department of Civil and Coastal Engineering, University of Florida.

Consolazio, G.R., Cowan, D.R., 2003. Nonlinear analysis of barge crush behavior and its relationship to impact resistant bridge design. Computers & structures 81 (8-11), 547-557.

Consolazio, G.R., Cowan, D.R., 2005. Numerically efficient dynamic analysis of barge collisions with bridge piers. Journal of Structural Engineering 131 (8), 1256-1266.

Cowan, D.R., Consolazio, G.R., Davidson, M.T., 2015. Response-spectrum analysis for barge impacts on bridge structures. Journal of Bridge Engineering 20 (12), 04015017.

Fan, W., Liu, Y., Liu, B., Guo, W., 2016. Dynamic Ship-Impact Load on Bridge Structures Emphasizing Shock Spectrum Approximation. Journal of Bridge Engineering 21 (10), 04016057.

Fan, W., Yuan, W., 2014. Numerical simulation and analytical modeling of pile-supported structures subjected to ship collisions including soil–structure interaction. Ocean Engineering 91, 11-27.
Institution, B.S., 2004. Eurocode 2: Design of Concrete Structures: Part 1-1: General Rules and Rules for Buildings. British Standards Institution.
Kang, L., Magoshi, K., Ge, H., Nonaka, T., 2017. Accumulative response of large offshore steel bridge under severe earthquake and ship impact due to earthquake-induced tsunami flow. Engineering Structures 134, 190-204.
Kulzep, A., Peschmann, J., 1999. Side Collision of Double Hull Tankers [Seitenkollision von Doppelhüllenschiffen]. Final Report of Life Cycle Design, Part D2A, Hamburg University of Technology.
Liu, B., 2017. Analytical method to assess double-hull ship structures subjected to bulbous bow collision. Ocean Engineering 142, 27-38.
Minorsky, V., 1958. An analysis of ship collisions with reference to protection of nuclear power plants. Sharp (George G.) Inc., New York.
Norsok, N., 2004. 004, Design of steel structures. Standards Norway, Rev 2.
Norsok Standard, N., 2007. 003. Actions and Action Effects, Edition 2.
Pedersen, P.T., Valsgaard, S., Olsen, D., Spangenberg, S., 1993. Ship impacts: bow collisions. International Journal of Impact Engineering 13 (2), 163-187.
Schwer, L.E., 2016. Modeling Pre and Post Tensioned Concrete 14th International LS-DYNA Users Conference.
Sha, Y., Amdahl, J., 2016. Design of Floating Bridge Pontoon subjected to Ship Collision, The 7th International Conference on Collision and Grounding of Ships.
Sha, Y., Hao, H., 2012. Nonlinear finite element analysis of barge collision with a single bridge pier. Engineering Structures 41, 63-76.
Sha, Y., Hao, H., 2013. Laboratory tests and numerical simulations of barge impact on circular reinforced concrete piers. Engineering Structures 46, 593-605.
Sha, Y., Hao, H., 2015. Laboratory tests and numerical simulations of CFRP strengthened RC pier subjected to barge impact load. International Journal of Structural Stability and Dynamics 15 (02), 1450037.
Storheim, M., Amdahl, J., 2014. Design of offshore structures against accidental ship collisions. Marine Structures 37, 135-172.
Storheim, M., Amdahl, J., 2017. On the sensitivity to work hardening and strain-rate effects in nonlinear FEM analysis of ship collisions. Ships and Offshore Structures 12 (1), 100-115.
Sun, B., Hu, Z., Wang, G., 2015. An analytical method for predicting the ship side structure response in raked bow collisions. Marine Structures 41, 288-311.
Tabri, K., Broekhuijsen, J., Matusiak, J., Varsta, P., 2009. Analytical modelling of ship collision based on full-scale experiments. Marine Structures 22 (1), 42-61.
Travanca, J., Hao, H., 2014. Numerical analysis of steel tubular member response to ship bow impacts. International Journal of Impact Engineering 64, 101-121.
Vrouwenvelder, A., 1998. Design for ship impact according to Eurocode 1, Part 2.7. Ship collision analysis, 123-134.
Woisin, G., 1980. Design against collision. GKSS-Forschungszentrum.
Yuan, P., 2005. Modeling, simulation and analysis of multi-barge flotillas impacting bridge piers.
Yuan, P., Harik, I.E., 2008. One‐Dimensional Model for Multi‐Barge Flotillas Impacting Bridge Piers. Computer‐Aided Civil and Infrastructure Engineering 23 (6), 437-447.
Yuan, P., Harik, I.E., 2009. Equivalent barge and flotilla impact forces on bridge piers. Journal of Bridge Engineering 15 (5), 523-532.